

Article

Design and Analysis of a Clutched Parallel Elastic Actuator

Bernhard Penzlin ^{1,*} , Mustafa Enes Fincan ¹ , Yinbo Li ² , Linhong Ji ² ,
Steffen Leonhardt ¹  and Chuong Ngo ¹ 

¹ Chair for Medical Information Technology, Helmholtz Institute, RWTH Aachen University, Pauwelsstr. 20, D-52074 Aachen, Germany

² Institute of Mechanical Design, Department of Mechanical Engineering, Tsinghua University, Shuangqing Road 30, Beijing 100084, China

* Correspondence: penzlin@hia.rwth-aachen.de; Tel.: +49-241-80-23514

Received: 24 July 2019; Accepted: 3 September 2019; Published: 5 September 2019



Abstract: Various actuator topologies are discussed for the purpose of powering periodic processes and particularly walking robots. The Clutched Parallel Elastic Actuator (CPEA) is proposed to reduce the energy consumption of active exoskeletons. A nonlinear model of the CPEA is presented in addition to the mechanical design. The CPEA prototype is operated with a passive load on the walking trajectory of the hip joint. The actuator is controlled with a cascaded position control and a superimposed Iterative Learning Controller (ILC). The controller was chosen to ensure comparability between active and deactivated spring operation. The application of the CPEA has the potential to increase efficiency in the design of exoskeletons.

Keywords: parallel-elastic actuators; energy-efficient actuators; compliant actuators; rehabilitation robotics; actuator design

1. Introduction

The use of compliant actuators is often associated with safe human–machine interaction, the reduction of peak torque, peak power, and energy consumption [1–3]. Actuators with additional elasticity activatable via a clutch, as an extension of the actuators with constant, permanently-engaged springs, are moving into focus [4]. Various approaches for using parallel elastic actuators (PEAs) have been introduced. Minimizing power consumption for the performance of periodic tasks is of great interest. A possible option for this is the addition of Parallel Elasticities (PEs). This applies generally to robots and particularly to all automated applications where a proper torque-angle profile is to be achieved. It was shown in an experiment with a Clutched PEA (CPEA) for use on a robot that the efficiency of the drive can be increased by 55%, whereby the comparison system recuperates the energy electrically [5]. The application of PEAs in prosthetics has already proven successful with prototypes. The interaction between human and machine can be improved by optimizing the stiffness and foot alignment to the walking situation [6]. Grimmer et al. showed in a simulation study that the energy consumption and the peak power are reduced by a PEA for the ankle joint over a range between 0.5 m/s and 2.6 m/s [7].

Furthermore, there are prototypes including a PE that support the knee [8]. Liu et al. developed a switching PEA, where the PE is activated in the stance phase to recycle energy and support the body weight, especially for the stance phase of robot legs during running. The actuator is designed for the knee, and it is not a motion support system for humans [9]. A PEA for the hip was also presented for force enhancement and support in industrial applications [10]. The PEAs are particularly interesting for active orthoses and exoskeletons of the lower limb, since the most important task, the upright gait,

is a periodic process. It has been demonstrated simulatively that the Root Mean Squared (RMS) power consumption can be reduced by up to 61% by the insertion of PEs. At the same time, the drive torque provided by the active part of the actuator decreases by up to 66% [11]. This can result in smaller actuators and batteries. There are further independent experimental results confirming the reduction of energy consumption by PEs during gait [12,13].

A disadvantage of the PEA is that it can have a negative effect on the energy requirement in the case of a non-cyclical positioning task. This can be bypassed by the switchable deactivation of the elasticity or by a dynamic adjustment of the equilibrium point [14].

It is important for the design of an actuator to know which torques and speeds are to be assumed. Maximum torques for the knee, normalized with the subject's weight, are set to 0.86 Nm/kg at a gait speed of 1.6 m/s [15]. The maximum normalized knee torque at gait speeds of around 1.2 m/s is 0.38 Nm/kg–0.56 Nm/kg depending on the posture. Under the same conditions, the normalized hip torque varies from 0.82–0.94 Nm/kg [16]. Actuators for hip support have been developed elsewhere [17–23]. Table 1 summarizes the existing design for hip actuators, including PEA, RA (Rigid Actuator), SEA (Serial Elastic Actuator), cRSEA (clutched Rigid Series Elastic Actuator), and MAACEPA. In the summary, the torque at 100% support is between 18 Nm and 68.6 Nm, and the nominal velocity is between 25 rpm and 84.7 rpm. So far, no actuator prototype has been published that is designed as a CPEA for full support in hip rehabilitation.

Table 1. Overview: actuators for supporting the hip motion (* marks 30 % torque support).

Topology	Power	Rated Torque	Velocity	Spring Rate	Purpose	Ref.
PEA	100 W	28.9 Nm	37.4 rpm	8 Nm/rad	Industrial	[17]
MACCEPA	50 W	11.2 Nm *	28 rpm	28.1 to 81.4 Nm/rad	Sit-to-stand	[18]
SEA	90 W	40 Nm	25 rpm	123 Nm/rad	Walking	[19]
cRSEA	200 W	18.2 Nm	84.7 rpm	Energy buffer/torque sensor	Walking	[20]
RA	100 W	34 Nm	25 rpm	Not applicable	Walking	[21]
RA	355 W	40.5 Nm	75 rpm	24 kNm/rad	Walking (0.2 m/s)	[22]
RA	150 W	68.6 Nm	36.3 rpm	Not applicable	Walking	[23]

An actuator is presented in this paper that has been designed for the hip joint of an exoskeleton or active orthosis. The hypothesis of this paper is that energy demand and peak load values can be reduced by using a PEA at the hip. The second section of this paper presents the CPEA with its functional structure, a model, and the prototype developed. In the third section, the actuator control including cascaded and iterative learning control are explained. In the fourth section, the procedure for the experimental validation for a step response and gait trajectories of the hip is presented. Subsequently, the experimental results are discussed. The paper closes with a conclusion.

2. Mechanical Design

2.1. Technical Requirements

The CPEA is designed for the hip actuation of an exoskeleton or active orthosis in the sagittal plane. The hip has a range of motion from -10° extension to 30° flexion in normal gait, and the drive must, therefore, cover a range of 40° . Furthermore, for the safety of the test person, the joint should be equipped with a hard stop within the physiological range of motion [24]. Visual3D was used in experiments with healthy volunteers at slow walking speeds on a treadmill. Figure 1 depicts the torque standardized to the body weight and the speed of the hip at a gait speed of 1.1 km/h, where a 0% gait cycle corresponds to the heel strike. One stride is divided into 40% swing phase and 60% stance phase. These data were recorded from a gait experiment with a healthy volunteer in the motion lab and post-processed with Visual3D. In a stride cycle at that speed, the standardized torque stays below 0.25 Nm/kg, and the maximum speed stays below 2.5 rad/s. Although the maximum torque and the maximum speed do not occur at the same time, the actuator should, therefore, provide at least 120 W

of output power, assuming a body weight of 75 kg. These specifications also correspond to the values in Table 1.

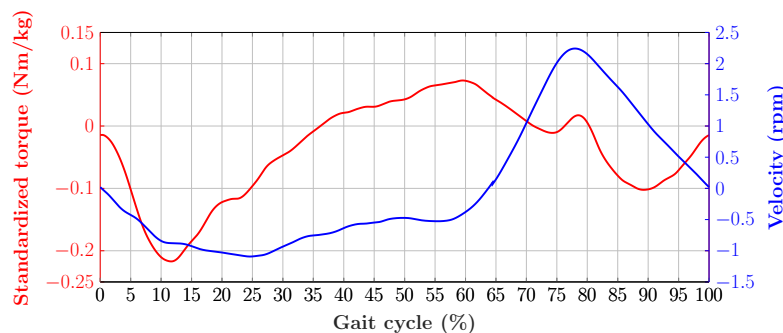


Figure 1. Measurement of a healthy volunteer: standardized torque and speed of the hip during the gait at 1.1 km/h.

The springs for gait support must be exchangeable. The design and spring selection should allow a maximum spring stiffness of at least 50 Nm/rad. Even if for a slower gait velocity, for example 1.1 km/h, lower spring rates are optimal, the larger values are potentially intended to support a faster speed or heavier subjects [11].

In contrast to knee and ankle actuators, a hip actuator does not significantly increase the mass moment of inertia during the swing phase, because it is connected to the torso. In the stance phase, the change in the mass moments of inertia of the individual limbs related to the test person's body mass is smaller [25,26]. The mass should be kept as low as possible, although the gearbox and motor are typically responsible for almost 2 kg of actuator weight. The hip actuators are more disturbing during the swinging of the arms in comparison to the two other joints. Therefore, the actuator should be as flat as possible, since this enlarges the width of the test person. An axial length of 100 mm is desired for clinical use, to allow the user to pass through doors and walk with crutches [15].

2.2. Structure Designed

The actuator designed is shown in Figure 2. All important components are numbered consecutively and will be described in the following section. The core task of the actuator is to convert electrical energy into mechanical energy. To fulfill this task, an EC90 Flat Frameless with a 260 W (1) (Maxon Motor AG, Sachseln, Switzerland) motor was chosen. The motor torque is transmitted via the drive shaft (2) to the wave generator (input) of the Harmonic Drive gearbox. The motor can provide a torque of about 1 Nm in rated operation. The gearbox and the engine are connected via the joint connection part (8), and the test bench mount is also mounted here. The load connection (5) for the test bench is connected directly to the output of the gear unit (6). The gearbox is a Harmonic Drive HFUS-2SO with a reduction ratio of 50:1 (6) (Harmonic Drive AG, Limburg an der Lahn, Germany). The load-side crossed roller bearing can subsequently be employed directly as a joint bearing for an exoskeleton (static load rating of 22 kN, maximum axial load of 5150 N, maximum tilting torque of 515 Nm) [27]. An adjustable end position limitation (7) is integrated into the actuator. This allows a swivel range of 120° in the version for the exoskeleton. The swivel range can also be changed by replacing the end position discs. Conventional coil springs (9) with a spring rate ranging from 1.8 N/mm–11.9 N/mm were used to realize the PE. The springs are connected to the cable drum (4) with a wire cable. The springs are extended to half of their maximum length in a neutral position, as this provides the largest swivel range. The lifting armature of the bistable magnet (3) fixes the ratchet disc and the cable drum (4) in a certain position to define the zero position of the springs. A short current pulse is required to fix the springs, and no additional current is needed to maintain the fixation due to the bistable magnet.

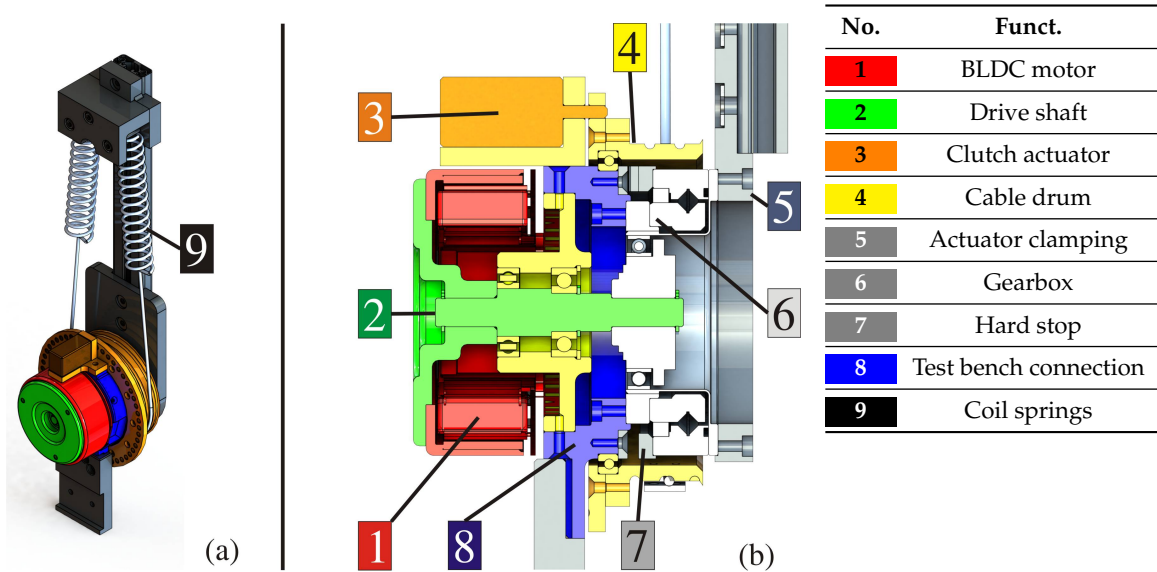


Figure 2. Images of a CPEA generated by computer-aided design: (a) Actuator in configuration for the test bench integration. (b) Sectional view of the actuator (without Parallel Elasticity (PE)).

2.3. Prototype

Figure 3 shows the prototype of the CPEA realized in a frontal and side view. In this configuration, a spring stiffness of about 30 Nm/rad was chosen (7). Further spring rates are conceivable, for example, when custom-made springs are used. The springs selected are from the standard product line of Gutekunst + Co. KG (Metzingen, Germany). The test bench connection is optional for connection to the test bench (5). The main components are numbered in the figure. An overview of the technical data of this CPEA is summarized in Table 2. An analytical model of the CPEA will be derived in the following subsection.

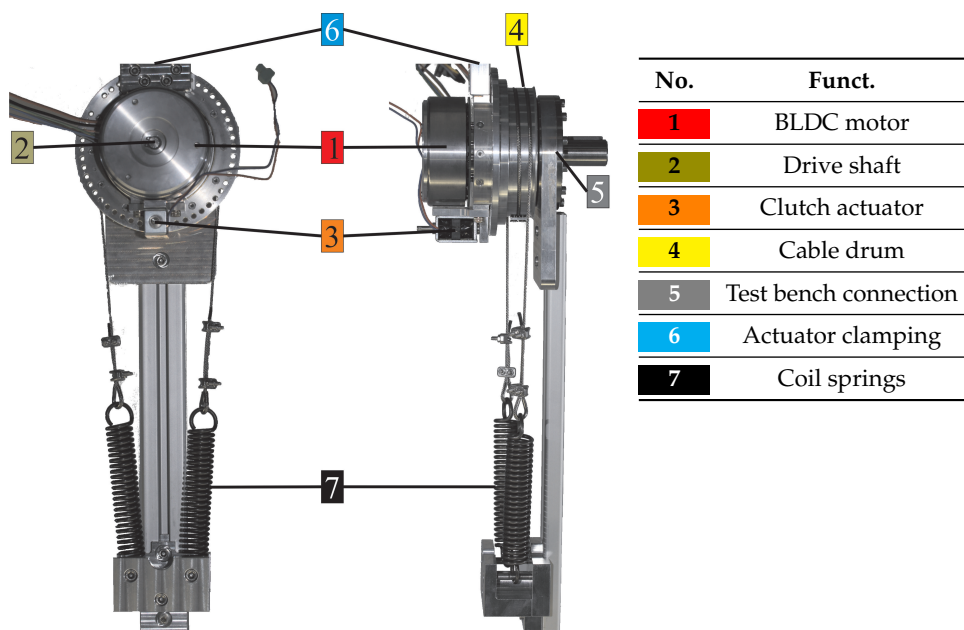


Figure 3. Photo of the completed prototype with the indication of the functionalities.

Table 2. Technical data of the Clutched Parallel Elastic Actuator (CPEA).

Specifications	Value
Nominal torque	49.4 Nm (active only)
Nominal speed	3.7 rad/s
No load speed	4.4 rad/s
Rated motor power	260 W (Maxon EC 90)
Mass	3.1 kg (including 30 Nm/rad springs)
Axial length	105 mm (including leg adapter)
Spring rate	10–67 Nm/rad (Mass: 50–360 g)
Spring type	Steel tension springs (EN 10270-1)
Clutch actuator	Bistable solenoid (30 W)

3. Modeling and Control

3.1. Modeling

A model with all the essential components was created for the simulation of the actuator and the design of the controllers. The motor was simulated as a current controlled torque source with the motor constant C_τ and the motor current i_m . The friction of the motor was modeled as the damping constant d multiplied by the rotational speed $\dot{\varphi}_m$. J_m is the moment of inertia of the motor. The torque on the input side of the gear unit is defined by:

$$\tau_{g,in} = C_\tau \cdot i_m - d \cdot \dot{\varphi}_m - J_m \cdot \ddot{\varphi}_m. \quad (1)$$

The gearbox is modeled by the efficiency curves given in the data sheet. There is a function here that defines the torque efficiency $K(\tau_{g,out})$. This function can be approximated according to the data of the Harmonic Drive by:

$$K(\tau_{g,out}) = (k_0 + k_1 \cdot V(\tau_{g,out}) + k_2 \cdot 10^{-k_3 \cdot V(\tau_{g,out})}), \quad (2)$$

where the torque factor V is defined by:

$$V(\tau_{g,out}) = \frac{\tau_{g,out}}{\tau_N} = \frac{\text{Torque (at output)}}{\text{Rated torque at rated speed}}. \quad (3)$$

The speed-dependent efficiency $\eta(\dot{\varphi}_m)$ can be approached by a third order polynomial. Speed efficiency and torque efficiency, Equation (2), functions are summarized as the nonlinear function:

$$f(\dot{\varphi}_m, \tau_{g,out}) = K(\tau_{g,out}) \cdot \sum_{i=0}^3 a_i \cdot \dot{\varphi}_m^i. \quad (4)$$

The coefficients a_i were determined using data from the gearbox manufacturer [27]. The input torque was multiplied directly by the reduction ratio r_g and then weighted according to the speed and torque-dependent efficiency. The mass moment of inertia of the gear unit J_g was applied to the output side of the drive. The output torque of the Harmonic Drive gear unit is, thus, defined by:

$$\tau_{g,out} = \tau_{g,in} \cdot r_g \cdot f(\dot{\varphi}_m, \tau_{g,out}) - J_g \cdot \ddot{\varphi}_l. \quad (5)$$

The PE is represented by its linear spring rate k_{PE} . The equilibrium position of the spring can be set at any position φ_{eq} . The spring is tensioned by a deflection of the load position φ_l from this equilibrium position. The spring torque is determined by:

$$\tau_{PE} = K_{PE} \cdot (\varphi_{eq} - \varphi_l). \quad (6)$$

The load is actuated by the sum of the gear output torque $\tau_{g,out}$ and the spring torque τ_{PE} .

Table 3. All parameters of the model including their name, symbol, and value.

Name	Symbol	Value
Rotor inertia	J_m	$5.300 \cdot 10^{-4} \text{ kg}\cdot\text{m}^2$
Torque constant	C_τ	0.136 Nm/A
Speed constant	C_ω	7.35 rad/Vs
Motor resistance	R_m	0.29 Ω
Motor inductance	L_m	$0.369 \cdot 10^{-3} \text{ H}$
Damping constant (motor)	d	$1.5 \cdot 10^{-5} \text{ Nm/rad}$
Spring rate (PE)	K_{PE}	30 Nm/rad
Equilibrium position	φ_{eq}	0.35 rad
Nominal torque (gearbox)	τ_N	25 Nm
Gearbox inertia	J_g	$1.93 \cdot 10^{-5} \text{ kg}\cdot\text{m}^2$
Reduction ratio	r_g	50:1
Coefficients (torque efficiency)	k_0	1.019
	k_1	-0.00765
	k_2	-0.849
	k_3	1.758
Coefficients (speed efficiency)	a_0	0.8776
	a_1	-0.0008136 s/rad
	a_2	$1.933 \cdot 10^{-6} \text{ s}^2/\text{rad}^2$
	a_3	$-2.289 \cdot 10^{-9} \text{ s}^3/\text{rad}^3$
Load inertia	J_{Load}	0.8 kg·m ²
Gravitational constant	g	9.81 m/s ²
Mass of the load	m	5 kg

3.2. Cascaded Control

A cascaded control structure, as shown in Figure 6, was applied to control the actuator. The innermost control loop was the current controller of the brushless DC motor. The electrical parameters of the motor are decisive for the design of the controller. This Proportional-Integral (PI) current controller was implemented on the ESCON 50/8 motor control unit of the EC90 Frameless (Maxon Motor AG, Sachseln, Switzerland) and ran at a sampling rate of 53.6 kHz. The speed controller was implemented on a real-time computer (MicroLabBox (MLB), dSPACE GmbH, Paderborn, Germany) system. In contrast to the PI current controller, the connected load also determines the design of the PI speed controller. The position controller was also implemented on the MLB. The system sampling rate on the MLB was set to 10 kHz. The model shown in Figure 4 was applied for speed and position control.

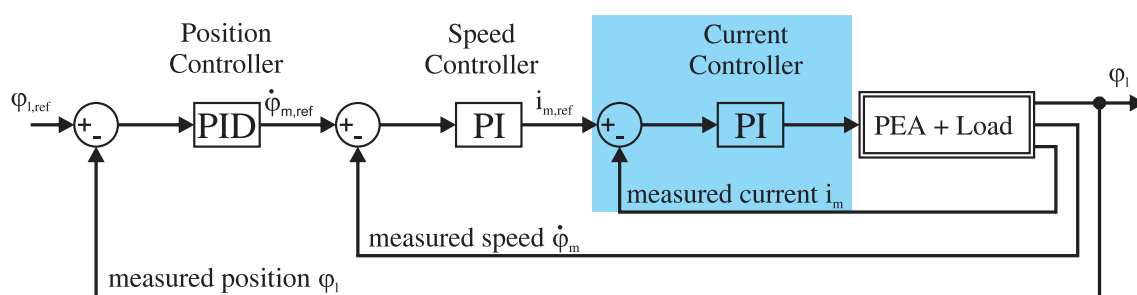


Figure 6. Cascaded control scheme. The current controller is implemented in the motor controller, which is marked with a blue area.

3.3. Iterative Learning Control

A superimposed controller must be implemented in addition to the cascaded control to ensure that the output trajectories match well with the reference values in any experiment. Since the human gait is a very periodic motion task, an ILC is recommended for a better trajectory matching in addition

to the cascaded control [28]. The control error was recorded for each cycle and reduced step by step by using the ILC [29]. It is possible to use the serial architecture of the ILC for experimental use with the cascaded controllers implemented in the motor control unit, as shown in Figure 7.

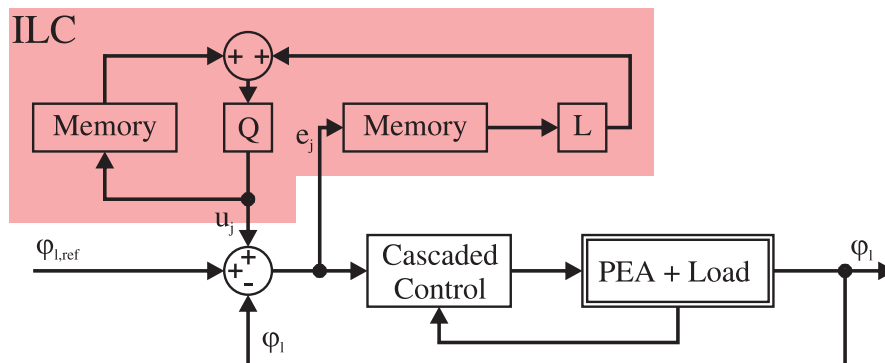


Figure 7. Position control consisting of an iterative learning controller (which is marked with a red area) in series with the cascaded feedback controller.

The filters $L(q)$ and $Q(q)$ are called the “learning function” and “Q-filter,” respectively. The ILC is defined by:

$$u_{j+1} = Q(q) \cdot [u_j(k) + L(q) \cdot e_j(k)] , \tag{9}$$

where k is the discrete time step in an iteration and $j \in \mathbb{N}_0$ is the iteration index. The controller inputs of the current and the last iteration are $u_{j+1}(k)$ and $u_j(k)$, respectively. q is the forward time-shift operator, which is defined as $q \cdot u(k) = u(k + 1)$. In our case, the learning function $L(q)$ was selected to be:

$$L(q) = l_0 + l_1 \cdot q. \tag{10}$$

The Q filter was neglected due to the noiseless digital encoder for the position and high inertia of the real load in the experiment. A forgetting factor γ can accelerate the convergence of the ILC [30]:

$$u_{j+1} = (1 - \gamma) \cdot u_j(k) + L(q) \cdot e_j(k). \tag{11}$$

4. Experiments

The step response of the cascaded system was recorded to examine the actuator with cascaded control. Two minutes of gait at 1.1 m/s on the treadmill were recorded in the motion laboratory. The data regarding the optimal spring from the paper by Wang et al. [11] were confirmed by evaluating the gait data in Visual3D (C-Motion Inc., Germantown, MD, USA). As a later input of the system, the positional progression of the hip joint was determined by a Fourier synthesis. This allows a periodic and reproducible reference sequence to be generated. We recall that any periodic function can be represented by a sum of weighted and shifted cosine signals in the form:

$$\varphi_{hip}(t) = \sum_{i=0}^k (m_i \cdot \cos(f_i \cdot t + \Delta\varphi_i)) . \tag{12}$$

Where m_i is the magnitude, f_i the frequency and $\Delta\varphi_i$ the phase shift. The determined parameters of the Fourier synthesis are listed in Table 4.

Table 4. The first seven frequencies, amplitudes, and phase shifts of the cosine envelopes for the periodic approximation of hip movement.

Number i	0	1	2	3	4	5	6
Frequency f_i	shift	0.47 Hz	0.95 Hz	1.42 Hz	1.90 Hz	2.37 Hz	2.85 Hz
Magnitude m_i	19.77°	24.47°	14.84°	5.53°	0.33°	1.16°	0.80°
Phase shift $\Delta\varphi_i$	0°	-39.16°	-88.16°	88.64°	61.51°	90.33°	29.73°

An averaged angle and torque trajectory from Visual3D measurement data was used to determine the spring and the preload angle optimally. The method of calculation was based on the procedure described by Wang et al. [11]. The torque and joint angle profile is shown in Figure 8. The joint torque of the hip in the sagittal plane is plotted over the angular position of the hip joint. To calculate the optimum spring for a complete gait cycle, the stiffness was obtained by linear regression [31]. The spring characteristic curve is defined by:

$$\tau_{spring}(\varphi) = K \cdot (\varphi - \varphi_{eq}). \quad (13)$$

The solution to Equation (13) was determined using the Curve Fitting Tool in MATLAB. For the gait data selected, the preload angle φ_{eq} was about 20° , and the spring rate was about $K = 30 \text{ Nm/rad}$. The spring determined is inserted into the profile in Figure 8.

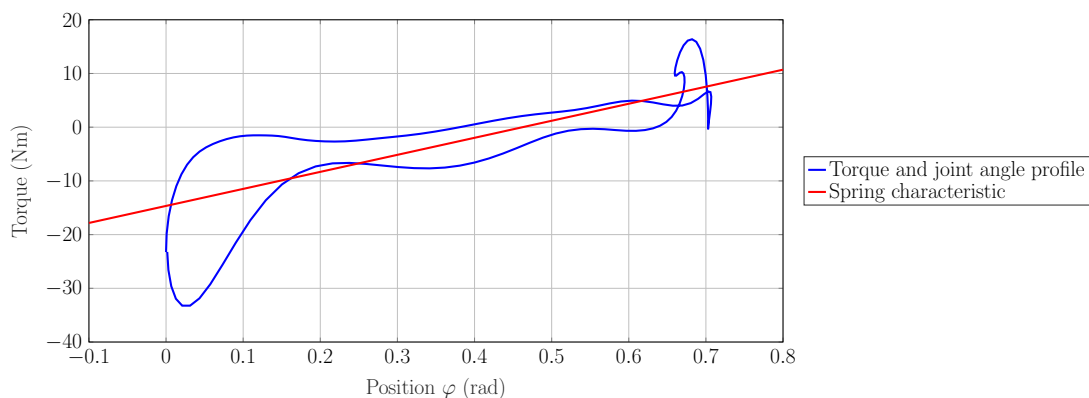


Figure 8. Measurement of a healthy volunteer: averaged torque and joint angle profile of the hip during a measured gait at 1.1 m/s and the spring characteristic determined.

The torque showed a hysteresis behavior in relation to the position φ . Some reasons for this phenomenon can be identified. For the hip, two arcs of motion can be observed. On the one hand, for the extension in the stance phase, the maximum extension was reached right before the swing phase. On the other hand, this is the swing phase in which the hip flexes [24]. As a result, the flexion and extension of the hip required an individual dynamic model. In stance and swing phase, maximum speed was approximately 1.2 rad/s and 2.3 rad/s respectively for a velocity of 1.1 km/h. Besides, the inertial torque was dependent on the acceleration and the current mass moment of inertia, which changed significantly during a gait cycle. This justifies why the torque characteristic showed the hysteresis behavior. Even if the tendency of the spring effect was nearly evident over the entire torque and joint angle profile, it could be argued why the coefficient of determination of the approximation was only 60.6%.

Experimental Setup

The test bench was set up according to the topology shown in Figure 9 to perform the experiments. The spring was deactivated or activated by the switching agent in the experiments; a self-made relay board was built for its control. Current and speed controllers were integrated into the motor controller. The MLB was selected to implement the superimposed position control and the ILC. The values measured were recorded via the connection between the computer and the MLB.

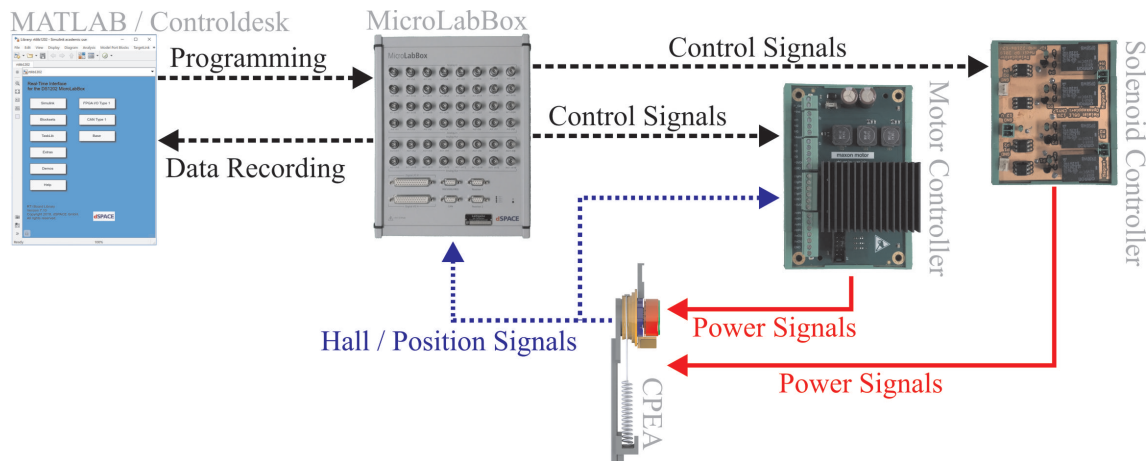


Figure 9. Schematic representation of the experimental setup.

The mechanical structure of the test bench during the experiments is shown in Figure 10. The actuator CPEA (motor (1) and the PE with clutch (2)) were attached to an aluminum profile frame. Actuator output (3) and shaft (5) were connected by an Oldham coupling (4). The CPEA cross-roller bearing was supplemented by a floating bearing (6) (bearing block PBT25, Misumi, Koto, Tokyo, Japan) close to the load. During the tests, the actuator was equipped with a load pendulum (7) with a lever arm of 0.4 m and a mass of 5 kg, and the mass moment of inertia was $J = 0.8 \text{ m}^2 \cdot \text{kg}$, an approximation of the leg in the swing phase, when the thigh and the lower leg were considered as point masses [25].

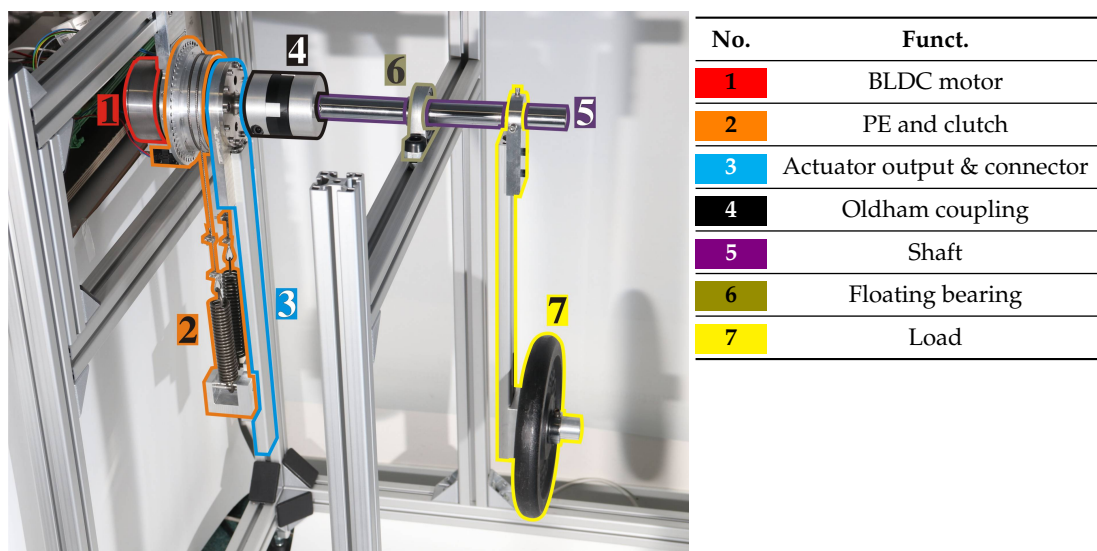


Figure 10. Configuration of the test bench with mounted CPEA and load.

Figure 10 shows the test bench with mounted CPEA and load. Figure 11 shows the load at different positions (0° , 10° , 20° , and 30°) during the experiment. One of the two coil springs was visible at this angle, and the greatest elongation in this experiment was only about half of the maximum

allowed elongation of the spring. By reducing the diameter of the cable drum of the actuator, the range of rotation would increase, so that the spring constants would decrease.

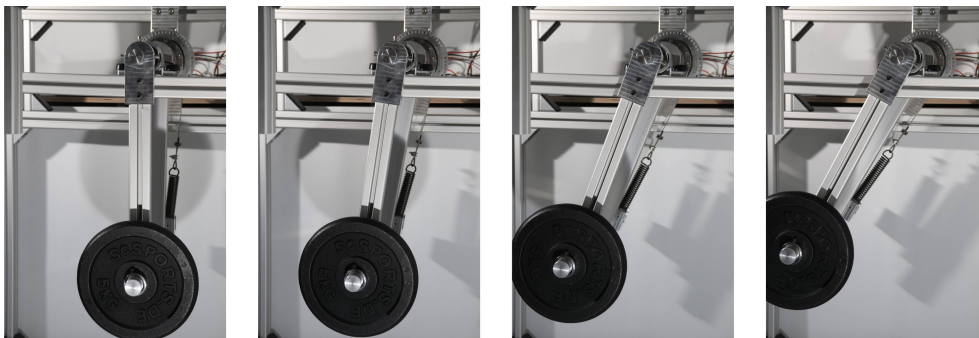


Figure 11. Photo sequence of the experiments. Range of motion: 0° – 30° .

5. Results and Discussion

The results of the step response and the controlled operation with a hip trajectory for 1.1 m/s follow. The ILC was only applied to the gait trajectories. For the step response, the cascaded control was applied as it was not a cyclic task. First, the step response is shown in Figure 12.

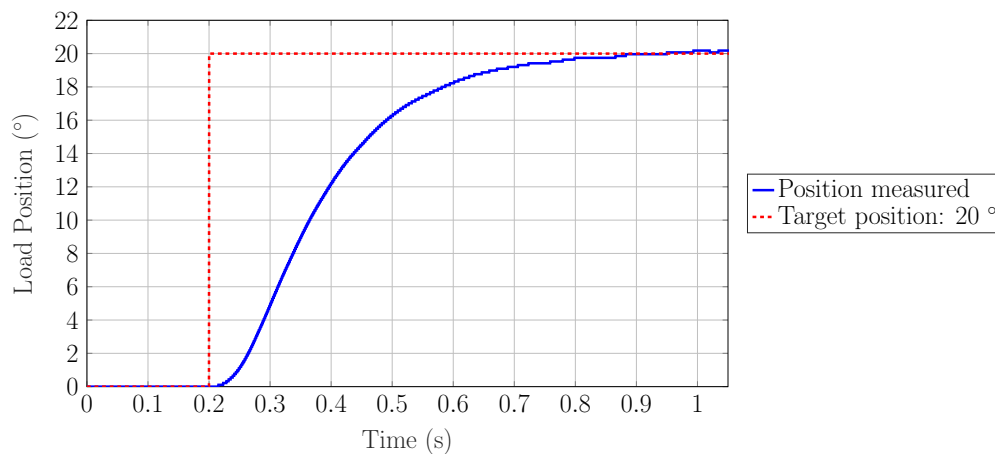


Figure 12. Step response of the CPEA with a pendulum load.

The set point was reached after about 0.6 s with an input step of 20° to the cascaded controlled actuator without parallel springs. The motor allowed a 13-fold current overload at start-up, and the collision torque of the gearbox was 98 Nm. For the safety of the gearbox, the over-current in the motor controller was limited accordingly to 8 A (twice the nominal value). The maximum torque of the motor limited the minimum response time. In the next paragraph, the experiments with reference trajectories of the hip are presented.

The angular course of the ILC-controlled actuator with PE and without elasticity was shown in this experiment, while they can hardly be separated in Figure 13. The ILC did not work in the first cycle; therefore, the control deviation was larger. Since the load is a pendulum, and thus a non-linear load (see Equation (8)), the controller was optimized for a particular operating point. Without ILC, this can lead to larger control deviations if the operating point is changed. By readjusting the controllers, a better working cascaded controller could be found especially for this task. Adaptive adaptation of the controllers would improve the disturbance transfer function in a test environment with stochastic disturbances. The ILC achieved a highly similar system response for both configurations for this input function. As can be seen from the second cycle onwards in Figure 13, the error was reduced

significantly. The root mean square error (RMSE) was calculated to evaluate the improvement of the control error:

$$e_{RMS} = \sqrt{\frac{1}{n} \sum_n (\varphi_{ref} - \varphi_l)^2}, \quad (14)$$

where $n = 13,247$ is the number of measurement samples during one gait cycle. The iterative improvement of the RMSE during experiments is listed in Table 5.

Table 5. Iterative improvement of the RMS error of the load position achieved by the ILC.

Iteration	1	2	3	4	5	6	7
RMSE	6.48°	2.49°	1.65°	1.01°	0.53°	0.38°	0.26°

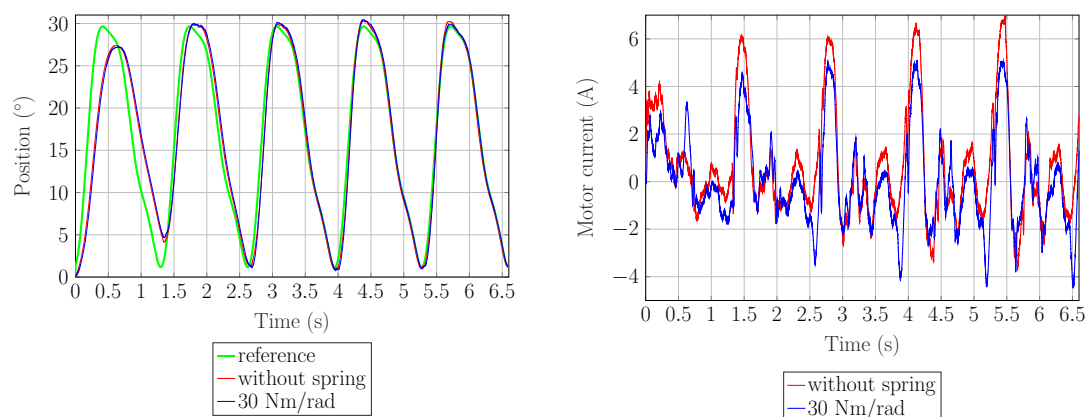


Figure 13. Comparison of PEA with a 30-Nm/rad spring (equilibrium position 20°) and rigid actuator. **Left:** the position trajectory for a reference of the hip; **right:** the motor current associated with the trajectory.

It should be noted that the angle discretization during the experiment was 0.11°. By comparing the RMS errors of both configurations, it can be shown that the angle profile can be compared with and without PE, since the motion task was executed with identical accuracy. Thus, different characteristic values for the actuator with and without PE can be compared directly.

The motor current and the motor torque are important selection parameters for an electric motor. Therefore the current is the first metric of our analysis. The peak current at the reference trajectory for the hip has been reduced from 7.0 A to 5.2 A in the experiment, as shown in Figure 13.

The motor power during the tests is shown in Figure 14. When dimensioning the motor, the maximum power consumption was another selection criterion. The maximum power consumption was reduced from 94.7 to 71.1 W (24%) for the hip reference trajectory. The average RMS power and the energy consumption per step were important for the dimensioning of the entire system with battery or power supply. The RMS power was reduced from 26.9 to 19.1 W (29%) by using PE. The quantity of energy per step was reduced from 18.4 to 14.9 Ws (19%). The PE in the motion tests with the hip trajectory on the test bench reduced all characteristic specification values significantly. To summarize, the relative improvements of the characteristic specification values are shown in Figure 15.

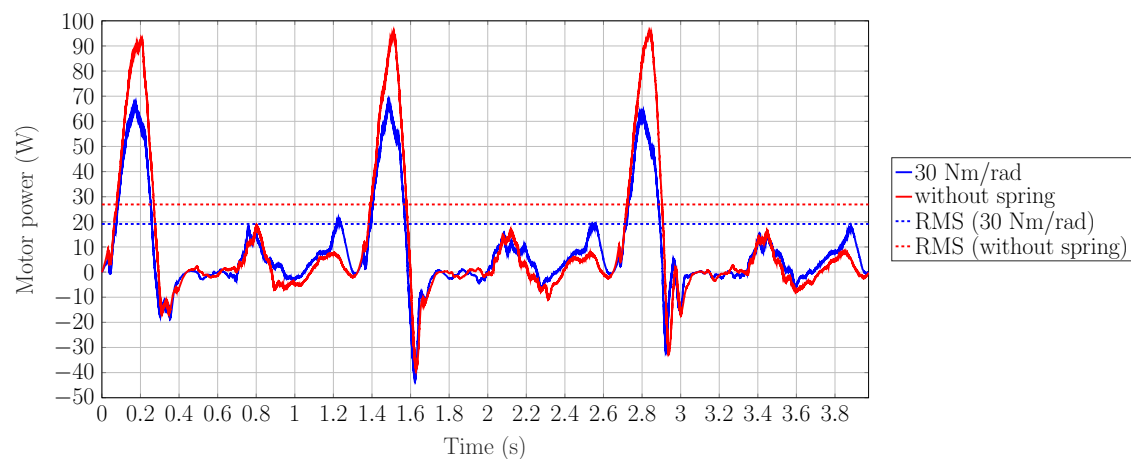


Figure 14. Motor power of the rigid actuator and PEA with 30 Nm/rad spring (Eq. Position 20°).

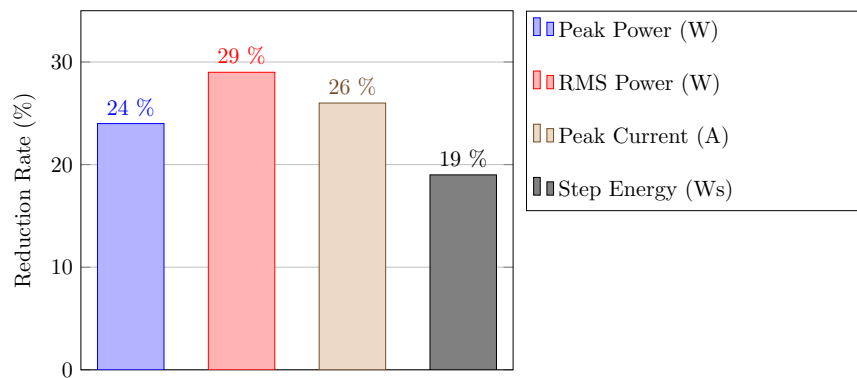


Figure 15. Reduction of the characteristic values due to the parallel elasticity, in a hip-like trajectory.

A reduction of the characteristic values was important in dimensioning the actuator, so that a smaller motor could be selected through this reduction and the gearbox could be designed smaller through the resulting reduced torques. In the long run, a portable power supply (battery) can be made smaller, potentially saving much weight in the overall design. A disadvantage that should be mentioned is that the mechanical spring with its mechanism was an extra weight compared to a rigid actuator. In our design, the additional weight due to the PE was between 380 and 690 g, depending on the spring rate desired. In order to give an impression of the component weight, the engine selected is available in a smaller configuration with about half the torque, which weighs 320 g less. This variation would at the same time reduce the axial length by 12 mm.

6. Conclusions

Our study confirmed that the CPEA reduced all characteristic specification values significantly (see Figure 15). A verification with direct human–machine interaction is still to be performed. Due to the fact that the elasticity can be deactivated, the actuator can also behave like a rigid actuator in non-periodic tasks, which excludes the disadvantages of a PEA here. The development of CPEA actuators seems promising due to the potential weight and consumption reduction for use in mobile rehabilitation robots. Development and research efforts are still needed to integrate CPEA drives into an exoskeleton and confirm the advantages of the actuator topology in studies with volunteers.

Author Contributions: Conceptualization, B.P.; data curation, B.P. and M.E.F.; formal analysis, B.P.; funding acquisition, L.J. and S.L.; investigation, B.P.; methodology, B.P.; project administration, B.P. and C.N.; resources, B.P.; software, B.P. and M.E.F.; supervision, B.P., L.J. and S.L.; validation, B.P. and M.E.F.; visualization, B.P.; writing, original draft, B.P.; writing, review and editing, B.P., Y.L. and C.N.

Funding: The research was funded by the joint Deutsche Forschungsgemeinschaft (DFG, German Research Foundation) and the National Natural Science Foundation of China (NSFC) project “Hybrid parallel compliant actuation for lower limb rehabilitation-HYPACAL” (LE 817/34-1) (NSFC 51761135121).

Conflicts of Interest: The authors declare no conflicts of interest. The funders had no role in the design of the study, in the collection, analyses, or interpretation of data, in the writing of the manuscript, nor in the decision to publish the results.

Abbreviations

The following abbreviations are used in this manuscript:

BLDC	Brushless Direct Current
CPEA	Clutched Parallel Elastic Actuator
ILC	Iterative Learning Control
MACCEPA	Mechanically-Adjustable Compliance and Controllable Equilibrium Position Actuator
MLB	MicroLabBox
PE	Parallel Elasticity
PEA	Parallel Elastic Actuator
PI Controller	Proportional-Integral Controller
PID Controller	Proportional-Integral-Derivative Controller
RA	Rigid Actuator
RMS	Root Mean Square
SEA	Series Elastic Actuator
cRSEA	Clutched Rigid Series Elastic Actuator

References

1. Ham, R.V.; Sugar, T.G.; Vanderborght, B.; Hollander, K.W.; Lefeber, D. Compliant actuator designs. *IEEE Robot. Autom. Mag.* **2009**, *16*, 81–94. [[CrossRef](#)]
2. Maciejasz, P.; Eschweiler, J.; Gerlach-Hahn, K.; Jansen-Troy, A.; Leonhardt, S. A survey on robotic devices for upper limb rehabilitation. *J. Neuroeng. Rehabil.* **2014**, *11*, 3. [[CrossRef](#)] [[PubMed](#)]
3. Jafari, A.; Tsagarakis, N.G.; Vanderborght, B.; Caldwell, D.G. A novel actuator with adjustable stiffness (AwAS). In Proceedings of the IEEE/RSJ International Conference on Intelligent Robots and Systems, Taipei, Taiwan, 18–22 October 2010; pp. 4201–4206.
4. Plooij, M.; Wolfslag, W.; Wisse, M. Clutched elastic actuators. *IEEE-ASME Trans. Mech.* **2017**, *22*, 739–750. [[CrossRef](#)]
5. Plooij, M.; van Nunspeet, M.; Wisse, M.; Vallery, H. Design and evaluation of the Bi-directional Clutched Parallel Elastic Actuator (BIC-PEA). In Proceedings of the IEEE International Conference on Robotics and Automation (ICRA), Washington State Convention Centre, Seattle, WA, USA, 25–30 May 2015; pp. 1002–1009.
6. Stuhlenmiller, F.; Schuy, J.; Beckerle, P.; Rinderknecht, S. A user-specific human-machine interaction strategy for a prosthetic shank adapter. *Curr. Dir. Biomed. Eng.* **2017**, *3*, 493–496. [[CrossRef](#)]
7. Grimmer, M.; Eslamy, M.; Gliuch, S.; Seyfarth, A. A comparison of parallel-and series elastic elements in an actuator for mimicking human ankle joint in walking and running. In Proceedings of the 2012 IEEE International Conference on Robotics and Automation, Saint Paul, MN, USA, 14–18 May 2012; pp. 2463–2470.
8. Roozing, W.; Li Medrano-Cerda, Z.; Gustavo, A.; Caldwell, D.; Tsagarakis, N. Development and control of a compliant asymmetric antagonistic actuator for energy efficient mobility. *IEEE-ASME Trans. Mech.* **2015**, *21*, 1080–1091. [[CrossRef](#)]
9. Liu, X.; Rossi, A.; Poulakakis, I. A Switchable Parallel Elastic Actuator and its Application to Leg Design for Running Robots. *IEEE-ASME Trans. Mech.* **2018**, *23*, 2681–2692. [[CrossRef](#)]
10. Masood, J.; Ortiz, J.; Fernández, J.; Mateos, L.; Caldwell, D. Mechanical design and analysis of light weight hip joint parallel elastic actuator for industrial exoskeleton. In Proceedings of the 2016 6th IEEE International Conference on Biomedical Robotics and Biomechatronics (BioRob), Singapore, 26–29 June 2016; pp. 631–636.

11. Wang, S.; Van Dijk, W.; Van der Kooij, H. Spring uses in exoskeleton actuation design. In Proceedings of the 2011 IEEE International Conference on Rehabilitation Robotics (ICORR), Zurich, Switzerland, 29 June–1 July 2011; pp. 1–6.
12. Mettin, U.; La Hera, P.; Freidovich, L.; Shiriaev, A. Parallel elastic actuators as a control tool for preplanned trajectories of underactuated mechanical systems. *Int. J. Robot. Res.* **2010**, *29*, 1186–1198. [[CrossRef](#)]
13. Li, Y.; Li, Z.; Penzlin, B.; Tang, Z.; Liu, Y.; Guan, X.; Ji, L.; Leonhardt, S. Design of the Clutched Variable Parallel Elastic Actuator (CVPEA) for lower Limb Exoskeletons. In Proceedings of the 41st International Conference of the IEEE Engineering in Medicine and Biology Society (EMBC), Berlin, Germany, 23–27 July 2019; accepted.
14. Häufle, D.; Taylor, M.D.; Schmitt, S.; Geyer, H. A clutched parallel elastic actuator concept: Towards energy efficient powered legs in prosthetics and robotics. In Proceedings of the 4th IEEE RAS & EMBS International Conference on Biomedical Robotics and Biomechatronics (BioRob), Rome, Italy, 24–27 June 2012.
15. Cestari, M.; Sanz-Merodio, D.; Arevalo, J.; Garcia, E. An adjustable compliant joint for lower-limb exoskeletons. *IEEE-ASME Trans. Mech.* **2015**, *20*, 889–898. [[CrossRef](#)]
16. Lewis, C.; Sahrman, S. Effect of posture on hip angles and moments during gait. *Man. Ther.* **2015**, *20*, 176–182. [[CrossRef](#)] [[PubMed](#)]
17. Toxiri, S.; Calanca, A.; Ortiz, J.; Fiorini, P.; Caldwell, D.G. A parallel-elastic actuator for a torque-controlled back-support exoskeleton. *IEEE Robot. Autom. Lett.* **2017**, *3*, 492–499. [[CrossRef](#)]
18. Brackx, B.; Geeroms, J.; Vantilt, J.; Grosu, V.; Junius, K.; Cuyper, H.; Vanderborght, B.; Lefeber, D. Design of a modular add-on compliant actuator to convert an orthosis into an assistive exoskeleton. In Proceedings of the 5th IEEE RAS/EMBS International Conference on Biomedical Robotics and Biomechatronics, Sao Paulo, Brazil, 12–15 August 2014; pp. 485–490.
19. Zhang, T.; Tran, M.; Huang, H. Design and experimental verification of hip exoskeleton with balance capacities for walking assistance. *IEEE-ASME Trans. Mech.* **2018**, *23*, 274–285. [[CrossRef](#)]
20. Woo, H.; Na, B.; Kong, K. Design of a compact rotary series elastic actuator for improved actuation transparency and mechanical safety. In Proceedings of the 2017 IEEE International Conference on Robotics and Automation (ICRA), Singapore, 29 May–3 June 2017; pp. 1872–1877.
21. Önen, Ü.; Botsali, F.; Kalyoncu, M.; Tinkir, M.; Yilmaz, N.; Şahin, Y. Design and actuator selection of a lower extremity exoskeleton. *IEEE-ASME Trans. Mech.* **2013**, *19*, 623–632. [[CrossRef](#)]
22. Neuhaus, P.D.; Noorden, J.H.; Craig, T.J.; Torres, T.; Kirschbaum, J.; Pratt, J.E. Design and evaluation of Mina: A robotic orthosis for paraplegics. In Proceedings of the 2011 IEEE International Conference on Rehabilitation Robotics, Zurich, Switzerland, 29 June–1 July 2011; pp. 1–8.
23. Lee, S.; Sankai, Y. Power assist control for leg with hal-3 based on virtual torque and impedance adjustment. In Proceedings of the IEEE International Conference on Systems, Man and Cybernetics, Yasmine Hammamet, Tunisia, 6–9 October 2002.
24. Perry, J.; Burnfield, J. *Gait Analysis-Normal and Pathological Function*; Slack Inc.: Thorofare, NJ, USA, 2010; pp. 176–182.
25. De Leva, P. Adjustments to Zatsiorsky-Seluyanov’s segment inertia parameters. *J. Biomech.* **1996**, *29*, 1223–1230. [[CrossRef](#)]
26. Vallery, H.; Veneman, J.; Van Asseldonk, E.; Ekkelenkamp, R.; Buss, M.; Van Der Kooij, H. Compliant actuation of rehabilitation robots. *IEEE Robot. Autom. Mag.* **2008**, *15*, 60–69. [[CrossRef](#)]
27. Harmonic Drive AG. *Projektierungsanleitung Units HFUS-2UH/2SO/2SH*; Harmonic Drive AG: Limburg an der Lahn, Germany, 2014.
28. Nahrstaedt, H.; Schauer, T.; Hesse, S.; Raisch, J. Iterative Learning Control of a Gait Neuroprosthesis. *Automatisierungstechnik* **2008**, *56*, 494–501. [[CrossRef](#)]
29. Bristow, D.; Tharayil, M.; Alleyne, A. A survey of iterative learning control. *IEEE Control. Syst. Mag.* **2006**, *26*, 96–114.

30. Yang, H.; Li, S. PD-Type ILC Algorithm Research with Forgetting Factor for a Class of Linear Systems with Multiple Time Delays. *Appl. Mech. Mater.* **2012**, *220*, 1125–1130. [[CrossRef](#)]
31. Rouse, E.J.; Gregg, R.D.; Hargrove, L.J.; Sensinger, J.W. The difference between stiffness and quasi-stiffness in the context of biomechanical modeling. *IEEE Trans. Biomed. Eng.* **2012**, *60*, 562–568. [[CrossRef](#)] [[PubMed](#)]



© 2019 by the authors. Licensee MDPI, Basel, Switzerland. This article is an open access article distributed under the terms and conditions of the Creative Commons Attribution (CC BY) license (<http://creativecommons.org/licenses/by/4.0/>).